Silver Nanoparticle Synthesis Using an Inkjet Mixing System

Taisuke Maki*, Saki Takeda, Yosuke Muranaka and Kazuhiro Mae

Department of Chemical Engineering, Kyoto University, Kyoto, Japan

Individual nanoscale silver particles were produced using an inkjet mixing system. First, the behaviors of colliding droplets were investigated to prepare to conduct the synthesis without splitting merged droplets. When small droplets collided, they merged to form droplets that stayed in a state of coalescence at a higher discharging velocity. In addition, by changing the orientation at the collision point, the droplet velocity could be increased. Then, silver nanoparticle synthesis was conducted under conditions that avoided droplet splitting. Smaller particles were produced by higher-velocity collisions for all the examined droplet sizes. When droplets were 50–100 μm, an average particle diameter of 2.5 nm was produced. In addition, when droplets of different sizes collided, they formed a continuous supply of precursor, which subsequently resulted in production of particles with uniform size.

Keywords: silver nanoparticle, inkjet mixing system, microreactor, droplets, collision

INTRODUCTION

A micromixer is a small mixing device consisting of a channel with a width of less than a few hundred micrometers. Various types of mixers have been developed, from the simplest T-shaped, SAR mixer, which repeatedly divides and mixes fluid (Schwesinger et al., 1996; Fang and Yang, 2009), to the KM mixer, which divides fluid into extremely narrow channels and mixes the flows at one point (Nagasawa et al., 2005). In these microscale mixers, fluids have several unique characteristics (Hessel et al., 2005; Muranaka et al., 2017; Guo et al., 2020). Among the many advantages of micromixers, rapid mixing is the best. A rapid mixing device is a powerful tool for small particle synthesis because it can control particle nucleation and growth. According to the LaMer diagram, nucleation occurs instantly when the fluid concentration reaches the supercritical regime, and then nucleation and particle growth proceed in parallel (Mer, 1952). Therefore, precise control of reactant concentration by rapid mixing is the key for monodispersed particle synthesis. For example, Watanabe et al. successfully used a KM mixer to synthesize zeolitic imidazolate framework-8 nanoparticles (Watanabe et al., 2017). For more effective and precise nanoparticle synthesis, the following factors are important. The first factor is mixing speed. Because metal particle nucleation occurs very fast, within 1 ms (Takesue et al., 2011), a shorter mixing time is necessary for precise control. The second factor is the prevention of channel clogging. Because of the very small width of the micromixers, the produced particles easily stick to the wall and eventually cause clogging. To provide these important factors, an inkjet mixing system (IMS) was employed in this study, and the production of monodisperse silver nanoparticles was examined.

Recent inkjet technology is very developed. It is a highly reproducible method to continuously discharges droplets (under a picoliter) with precisely controlled amounts, orientation, velocity, and frequency. Therefore, the application of inkjet technology has spread from printing on paper to many industrial fields, such as 3D printing (Gupta et al., 2015), electronics (Yamada et al., 2016), and

FIGURE 1 | Conceptual diagram of the IMS apparatus. Nozzles were stabilized on the precisely orientation-controllable stages.

FIGURE 2 | Effect of the impact parameter on droplet orientation.
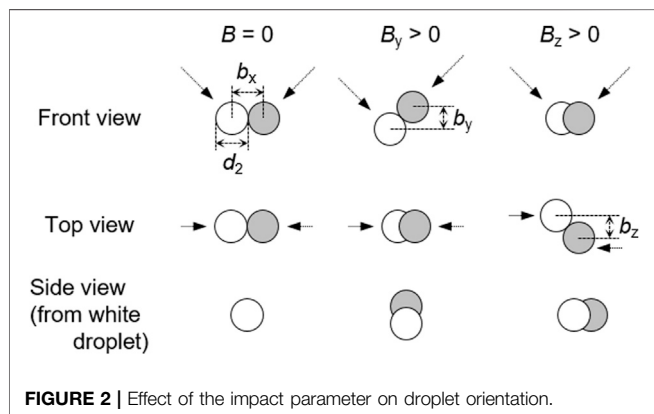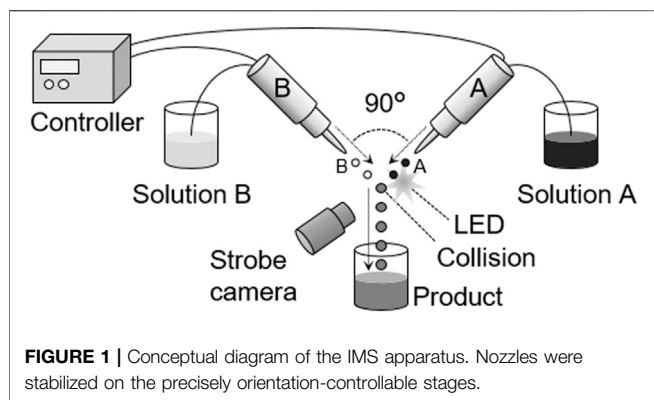
biomedicine (Mandrycky et al., 2016). This study demonstrates a new application of inkjet technology, which is the *in situ* synthesis of monodisperse nanoparticles. An inkjet system consists of two opposed inkjet nozzles and mixes small droplets in the air. Mixing occurs when particles collide and merge in air where there is no channel to be clogged. In addition, inkjet technology produces rapid mixing because the maximum diffusion length is limited in tiny droplets, and deformation/rotation due to collisions promotes mixing (Inohara et al., 2019). Davis et al. and Takano et al. reported that it was possible to mix two droplets in under 1 ms (Davis et al., 2017; Takano et al., 2015). Davis et al. achieved mixing in 200 μs by colliding 40 μm sized droplets. Furthermore, unlike conventional micromixers, IMS does not require a high flow rate for rapid mixing and can reduce reagent expenses. It is suitable for super high-value applications, such as medicines and cosmetics, to satisfy demands for small amounts of various products.

Silver nanoparticles (AgNPs) are a promising material with applications in catalysts, antibacterial agents, electronics, and optical devices. The production of monodisperse and size-controlled AgNPs is expected because there is an optimum particle size for each application. For example, dehydrogenation of alcohol was promoted most effectively by AgNP catalysts with an average diameter of 3.3 nm supported on hydrotalcite (Mitsudome et al., 2008a), and phenylsilane oxidation to silanol was catalyzed by 6–8 nm AgNPs supported on hydroxyapatite (Mitsudome et al., 2008b). In the

electronics field, a fine wiring method is being developed to produce ink containing AgNPs. The properties of AgNP ink depend on the particle size; for example, smaller particles result in lower electrical resistance and lower sintering temperature (Chen et al., 2009). In particular, a lower sintering temperature is important for preventing the deterioration and deformation of circuit boards. For use in optical devices, smaller particles enhance localized surface plasmon resonance for anticipated applications in the development of sensors and equipment to generate solar power (Scholl et al., 2012). AgNP production by liquid phase reduction using a micromixer has been examined; however, clogging was an obstacle (Baber et al., 2015). Our group previously reported that IMS enabled rapid mixing and production of monodisperse lipid nanoparticles (Inohara et al., 2019). In the report, higher droplet velocity and orientation were proven to enhance mixing. This paper reports AgNP synthesis by IMS and examines the effects of droplet sizes, velocities, and orientation on AgNP size.

EXPERIMENTAL SECTION

Materials

$AgNO_3$ (0.1 mol/L), NaOH (1 mol/L), and powdered $NaBH_4$ were purchased from Fujifilm Wako Chemical (Japan). Polyvinyl alcohol (PVA) of M_w = 89,000–98,000 was purchased from Sigma-Aldrich (Japan). The AgNP precursor solution was prepared by dissolving PVA to 0.02 wt% at 80°C, cooling the solution to the room temperature, and dissolving $AgNO_3$ to 0.9 mmol/L. The role of PVA was to protect against particle aggregation. To prepare the reducing agent, $NaBH_4$ and NaOH were solubilized in deionized water to concentrations of 1.8 and 5.8 mmol/L, respectively.

Apparatus and Analysis

Figure 1 shows the conceptual diagram of the apparatus used in this study. The IMS apparatus (IJK-200 W) was fabricated by Microjet Corp (Nagano, Japan). Two opposed nozzles independently discharged small droplets, which collided and merged in the air. In this study, solution A was the AgNP precursor solution, and solution B was the reducing agent. AgNP nucleation and particle growth occurred in the merged droplets through reduction. The nozzles discharged droplets by a piezoelectric system, where piezoelectric elements changed their volumes according to the voltage. Each nozzle was installed on the xyz-axis movable stage, and the collision point and angle were oriented by moving the stages. The product, AgNP particles, were photographed by transmission electron microscopy (TEM) (JEM-1010, JEOL, Japan), and the particle sizes were measured from the TEM images using ImageJ (Schindelin et al., 2012).

Dimensionless Numbers

This study employs two dimensionless numbers, the Weber number We and impact parameter B. We is the ratio of the internal force and interfacial tension, which expresses the shape and deformation property of a droplet or bubble and is formulated as shown in **Eq. 1**, where ρ is the merged droplet density [kg/m³],
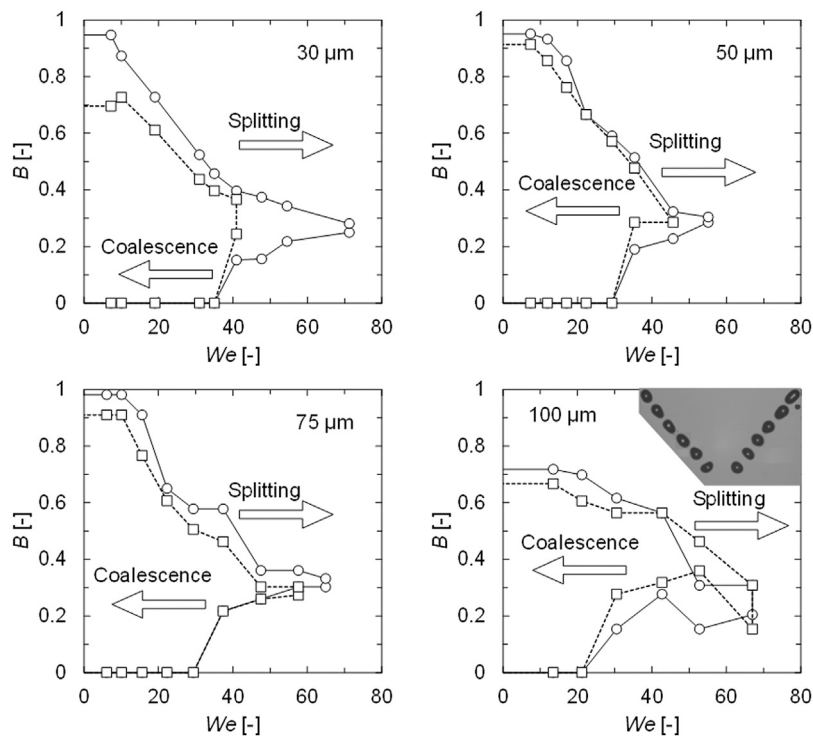
FIGURE 3 | Droplet coalescence and splitting behavior after collisions. Circle–$B_z > 0$, square–$B_y > 0$. The photograph on a scale of 100 μm shows the droplets before a collision.
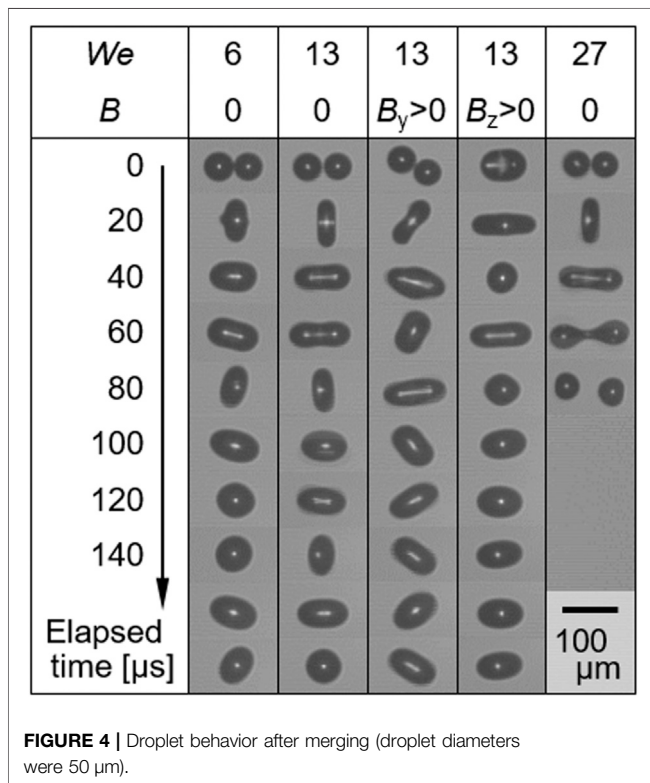
FIGURE 4 | Droplet behavior after merging (droplet diameters were 50 μm).

d_1 is the merged droplet diameter [m], u is the relative velocity of the colliding droplets [m/s], and σ is the interfacial tension [N/m]. B expresses the relative orientation of the droplets at the collision point and is formulated as shown in **Eq. 2**, where b is the separation of the centers of gravity of the droplets [m] and d_2 is the diameter of one of the droplets (AgNP precursor solution in this study) [m]. **Figure 2** illustrates the effect of B_i (i = y or z) on droplet orientation. In this study, B_x was not concerned because b_y and b_z can be controlled independently, however, b_x is dependent on the other b. When two droplets collide along a direct path, then B equals 0. B_y increases when solution B collides from the top side, where B_z increases when solution B collides horizontally but from the near side of the strobe camera.

$$We = \frac{\rho d_1 u^2}{\sigma} \qquad (1)$$

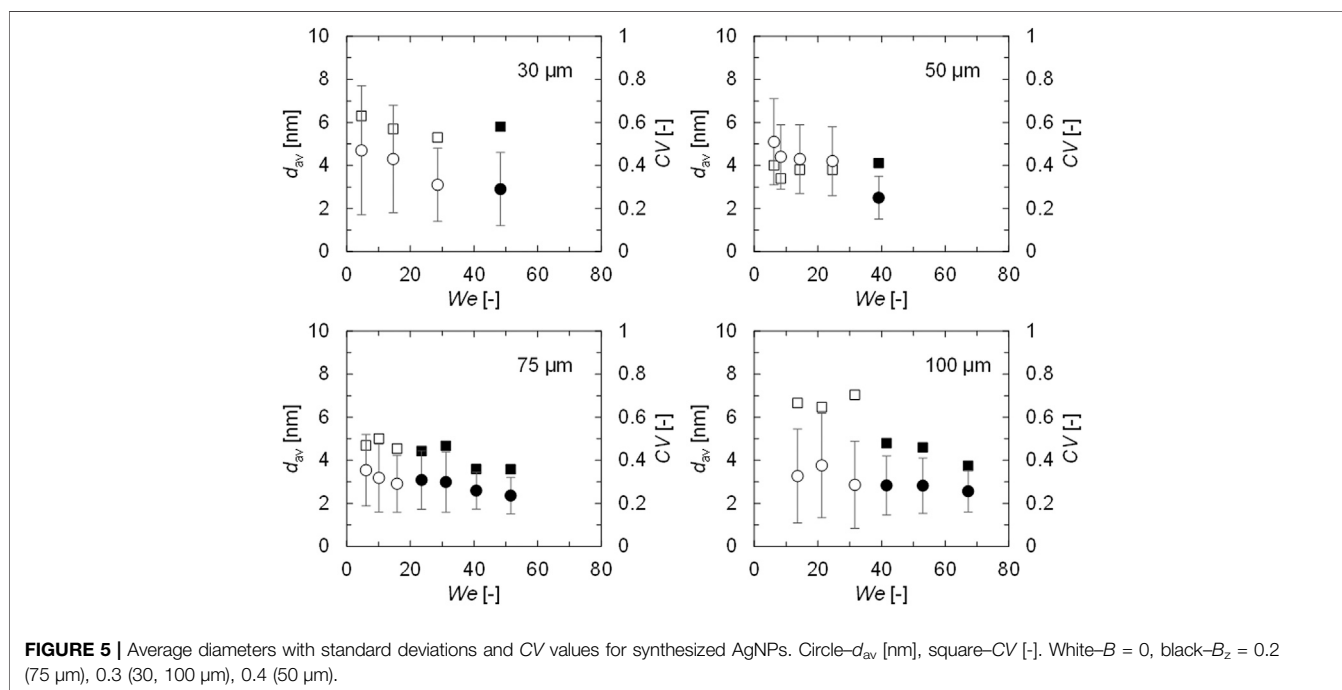$$B_i = \frac{b_i}{d_2} \qquad (2)$$

Experimental Conditions

Solution A and solution B were discharged from the opposed nozzles. The sizes and velocities of discharged droplets were 30–100 μm and 2.0–6.5 m/s, respectively, and both parameters were the same for solutions A and B. The frequency was 500 droplets/s. We was changed by altering the droplet size and velocity, while B was changed by moving the stages.

TABLE 1 | Brief summary of droplets conditions.

Discharged droplet diameter [μm]	Relative droplet velocity [m/s]	We [-]	B [-]
30	2.8–9.3	4.6–48.3	0 or B_z = 0.3
50	2.6–6.8	6.2–39.1	0 or B_z = 0.4
75	2.2–6.4	6.1–51.6	0 or B_z = 0.2
100	2.8–6.3	13.6–67.3	0 or B_z = 0.3

TABLE 2 | Brief summary of conditions for synthesis of droplets with different volumes.

Droplet diameter of solution a [μm]	Droplet diameter of solution B [μm]	Relative droplet velocity [m/s]	We [-]	Volume ratio [-]
50	80	4.2–7.1	21.5–59.7	B/A = 4.3
90	50	4.7–6.4	29.6–53.3	A/B = 6.0

FIGURE 5 | Average diameters with standard deviations and CV values for synthesized AgNPs. Circle–d_{av} [nm], square–CV [-]. White–B = 0, black–B_z = 0.2 (75 μm), 0.3 (30, 100 μm), 0.4 (50 μm).

RESULTS AND DISCUSSION

Behavior of Collided Droplet

Before the AgNP synthesis was examined, the behavior of the collided droplet was investigated using 30–100 μm water droplets at various We and B. When B_y was not 0, then B_z was set as 0, and vice versa. **Figure 3** shows a map of the coalescence and splitting of the collided droplets. For all the examined droplet diameters, the collided droplets remained coalesced for $B > 0$ in the high We region. In particular, by setting B_z at approximately 0.2, the collided droplets continued to coalesce at high We. With diameters of 30, 50, or 75 μm, the merged droplet did not split until $We < 30$–40 at $B = 0$ and until $We < 60$–70 at $B > 0$.
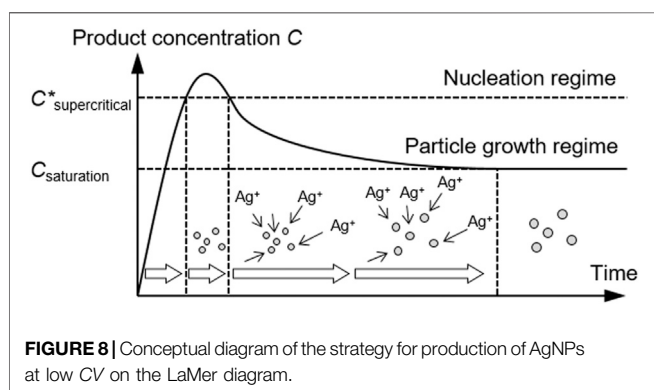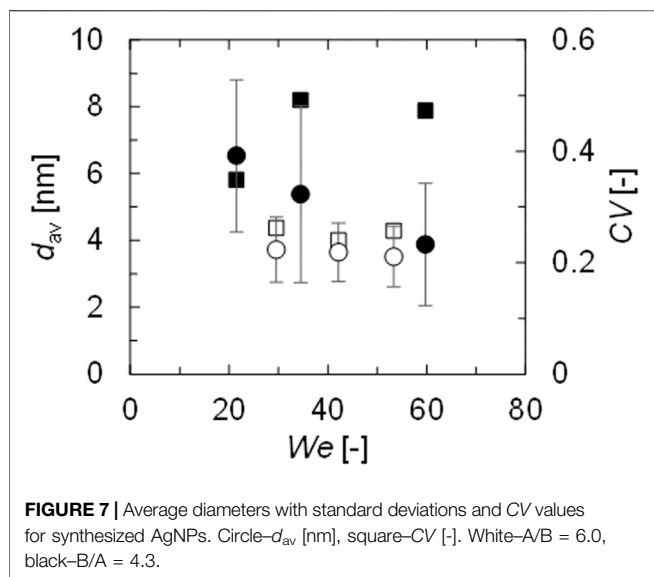
Therefore, it seemed that the coalescence/splitting behavior of the collided droplets could be predicted by We and B when the colliding droplet diameters were under 75 μm. Only 100 μm droplets had a different map in **Figure 3** because 100 μm droplets were not able to maintain a spherical shape even before the collision (as also shown in **Figure 3**). Regarding the mixing performance in the merged droplets, our group previously discussed this subject related to the production of lipid nanoparticles using an inkjet reactor (Inohara et al., 2019). The report revealed that mixing in a merged droplet was promoted by rotation around the horizontal axis (and not around the vertical axis), and this produced smaller monodisperse lipid nanoparticles. To promote horizontal

FIGURE 6 | Size distributions and TEM images of synthesized AgNPs.
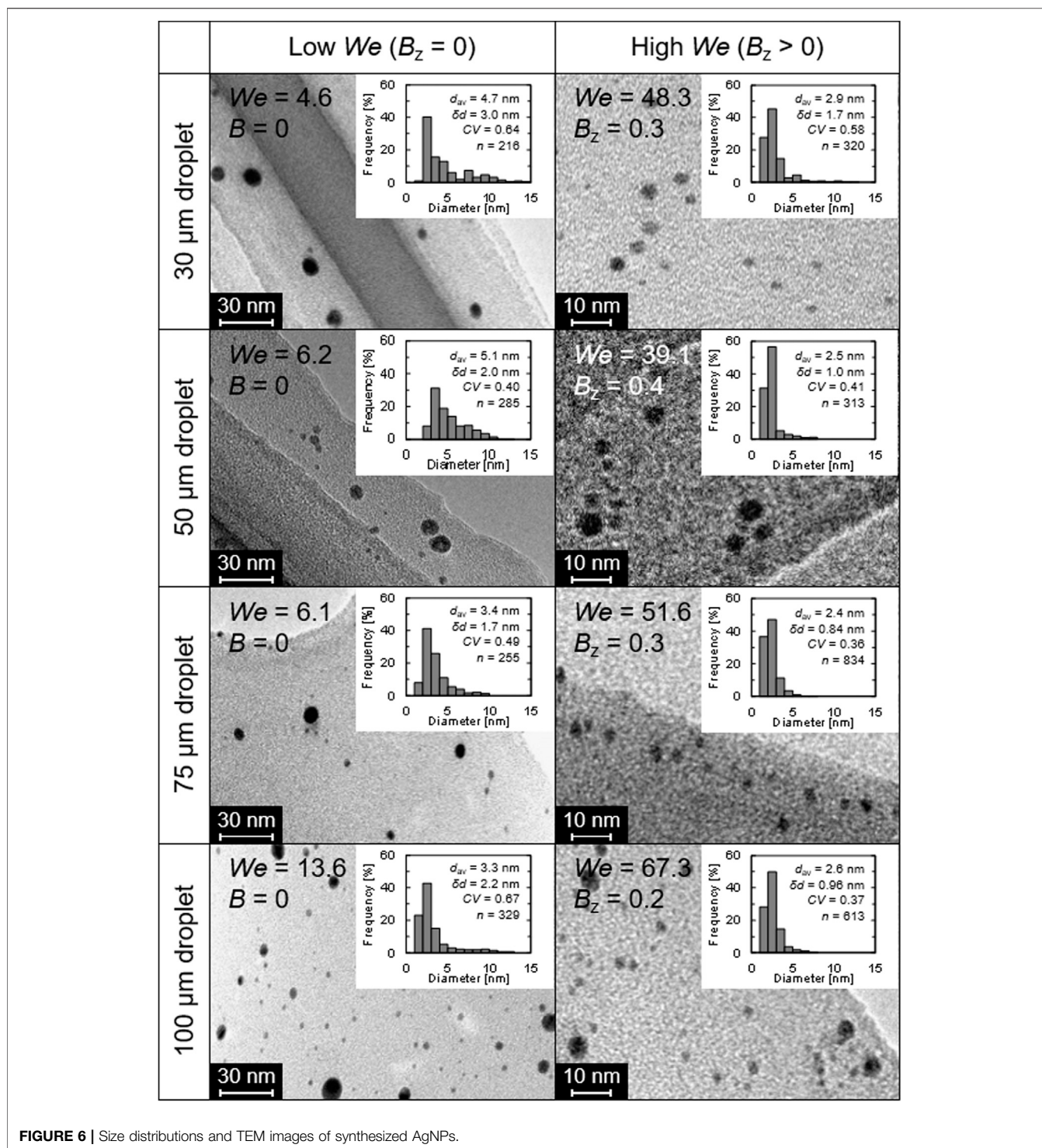
rotation, a value of $B_z > 0$ was important. **Figure 4** shows the behaviors of the merged droplets after 50 μm droplets collided at $We = 6-27$. Judging from the figure, horizontal rotation was promoted by increasing B_z from 0. According to these results and a previous report, AgNP synthesis was conducted under the (nonsplitting) conditions summarized in **Table 1** and detailed in **Supplementary Table S1**.

Synthesis of AgNPs

AgNPs were synthesized using IMS under the conditions determined in the previous section (listed in **Table 2**). It should be noted, that some of the result solutions were analyzed after 1 week, and the particle growth and aggregation in the collection vial were confirmed to be negligible. **Figure 5** shows the average diameter (d_{av}) and coefficient of variation (CV) of the synthesized

FIGURE 7 | Average diameters with standard deviations and *CV* values for synthesized AgNPs. Circle–d_{av} [nm], square–*CV* [-]. White–A/B = 6.0, black–B/A = 4.3.

FIGURE 8 | Conceptual diagram of the strategy for production of AgNPs at low *CV* on the LaMer diagram.

AgNPs. When droplet sizes were 50 µm, smaller AgNPs were synthesized at higher *We* with constant *CV*. By increasing *We*, mixing in the merged droplet was promoted, and small AgNPs were successfully synthesized. B_z enabled higher *We* and better mixing by rotation and resulted in d_{av} = 2.5 nm at *We* = 39.1. Baber et al. reported using a clog-free microfluidic impinging jet microreactor to synthesize very small AgNPs and obtained AgNPs that was approximately d_{av} = 4.1 nm at *We* = 65.0 (Baber et al., 2016). IMS enabled the synthesis of even smaller AgNPs, which indicated the significant potential of IMS. When discharged droplets were 30 µm, d_{av} and *CV* of synthesized AgNPs decreased with increasing *We*. However, *CV* was higher than the 50 µm droplet case at all examined *We* values, and the smallest d_{av} was also larger with a d_{av} of 2.9 nm at *We* = 48.3. This was because the inertial force was too low for droplets that were too small, which prevented the promotion of mixing. Generally, small droplets have the characteristics such as a high surface to volume ratio and the small diffusion length which result in the better mixing. However, in the significantly small scale, the physical properties such as the inertial force have larger effect than the macro scale (Wiktor et al., 2015). Therefore, the mixing

performance is on the balance between the factors such as the surface area to volume ratio, the diffusion length, and the inertial force. When the discharged droplets were 75 or 100 µm, d_{av} and *CV* of synthesized AgNPs also decreased with increasing *We*. At low *We*, 75 µm droplets (*We* = 6.1) resulted in AgNPs of d_{av} = 3.5 nm and *CV* = 0.47, while 100 µm droplets (*We* = 13.6) resulted in a smaller d_{av} of 3.3 nm and a higher *CV* of 0.67. Collisions of larger droplets promoted mixing due to higher internal forces at low *We*. However, a long diffusion lengths affected the mixing time distribution. At high *We*, 75 µm droplets (*We* = 51.6) resulted in AgNPs of d_{av} = 2.4 nm and *CV* = 0.36, while the larger 100 µm droplets (*We* = 67.3) resulted in a smaller d_{av} of 2.6 nm and a higher *CV* of 0.37. Judging from these results, mixing within the merged droplets was successfully promoted by high *We* with $B_z > 0$, and small AgNPs were synthesized regardless of the droplet size.

Next, the change in *CV* was discussed according to the TEM images. **Figure 6** depicts the TEM images and particle size distributions obtained with the highest *We* and lowest *We* for each droplet size. At low *We*, large AgNPs of approximately 10 nm were produced by all the examined droplet sizes. However, when the discharged droplets were larger, the proportion of the smaller AgNPs (such as 2–3 nm) increased; therefore, d_{av} was smaller despite the higher *CV* for larger droplets. When discharged droplets were small, *CV* was higher, even at high *We*. As discussed in the previous section, the low inertial forces on the small droplets decreased the mixing performance and produced a few large AgNPs that increased *CV*. Therefore, even though small AgNPs were produced with approximately d_{av} = 3 nm at high *We*, the *CV* value tended to increase with smaller droplets. In summary, IMS enabled AgNP production with d_{av} = 2.5 nm and *CV* = 0.4 under the condition of high *We* with $B_z > 0$ and 50–100 µm droplets. It should be mentioned that at this particle size scale, the *CV* value of 0.4 is notably low. For example, the percentage of product AgNP smaller than 5 nm was more than 90 % at the high *We* for all the droplet size cases, and except for the droplet of 30 µm the percentage was even more than 95%.

When the volumes of the collided droplets were the same, the *CV* value was approximately 0.4. According to the report by Baber et al., the *CV* of AgNPs produced by a microfluidic impinging jet reactor ranged from 0.2 to 0.3, which was notably low for the resulting AgNPs with a d_{av} of 4.1 nm. To lower the *CV*, the volume ratio of the droplets was changed. The colliding conditions were listed in **Table 2**. The concentrations of AgNP precursor ($AgNO_3$ and PVA) and reducing agent ($NaBH_4$ and NaOH) were prepared to be the same as for the merged droplets as the previous section, and *B* was 0 for all the conditions. B/A > 1 means that the larger proportion of dilute reducing agent solution B and the smaller proportion of concentrated silver precursor solution A collided, and A/B > 1 means that the larger proportion of dilute silver precursor A and the smaller proportion of concentrated reducing agent B collided. **Figure 7** shows the results. When the proportion of reducing agent solution B was larger, the *CV* values increased to approximately 0.5. In this case, solution A contained not only concentrated silver precursor of $AgNO_3$ but also concentrated Polyvinyl alcohol (PVA). Therefore, the particle protection by

PVA and the particle growth were more competitive than in the previous case, and some particles were immediately protected after nucleation, while others were continuously supplied with silver precursor, thus resulting in a higher *CV* value. However, when the proportion of silver precursor solution A was larger, the *CV* resulted in approximately 0.25, which was as low as the result by Baber et al. Under this condition, the silver precursor was pseudocontinuously supplied to the concentrated reducing agent. **Figure 8** illustrates the concept based on the LaMer model. At first, nucleation proceeded mildly at low precursor concentration, and concentration increased slowly to the supercritical regime. Subsequently, silver precursor was continuously supplied to the nuclei as mixing proceeded, keeping the concentration within the particle growth regime (supersaturation but below the supercritical regime, between $C_{saturation}$ and $C^{*}_{supercritical}$ in **Figure 8**). Thus, all the nuclei grew uniformly, and AgNPs were successfully produced with low *CV*.

CONCLUSION

IMS, which has the advantages of rapid mixing and no clogging, was used to produce individual nanoscale AgNPs. Prior to AgNP production, the behavior pattern of the collided droplets was investigated, and a coalescence-splitting map was compiled. By increasing the impact parameter B_z, which means colliding two droplets with horizontally displaced orientation, the collided droplets could stay merged at higher *We*. Thus, a high *We* was effective in producing smaller AgNPs for all examined droplet sizes. When the droplets were 50–100 μm, AgNPs of $d_{av} = 2.5$ nm were produced with a *CV* of approximately 0.4. In addition, the collision of droplets of different sizes resulted in a continuous precursor supply, which subsequently resulted in

production of AgNPs with low *CV*. Thus, the validity of the newly developed device was demonstrated.

DATA AVAILABILITY STATEMENT

The original contributions presented in the study are included in the article/**Supplementary Material**, further inquiries can be directed to the corresponding author.

AUTHOR CONTRIBUTIONS

TM proposed the idea of synthesizing nanoparticles using the inkjet mixing system and designed the apparatus, conducted instructive experiments, and gave advice as one of the supervisors. ST and YM conducted most of the experiments and analysis and summarized the article. KM gave much advice and many instructions as one of the supervisors.

FUNDING

SUPPLEMENTARY MATERIAL

The Supplementary Material for this article can be found online at: https://www.frontiersin.org/articles/10.3389/fceng.2021.742322/full#supplementary-material

REFERENCES

Baber, R., Mazzei, L., Thanh, N. T. K., and Gavriilidis, A. (2015). Synthesis of Silver Nanoparticles in a Microfluidic Coaxial Flow Reactor. *RSC Adv.* 5, 95585–95591. doi:10.1039/c5ra17466j

Baber, R., Mazzei, L., Thanh, N. T. K., and Gavriilidis, A. (2016). Synthesis of Silver Nanoparticles Using a Microfluidic Impinging Jet Reactor. *J. Flow Chem.* 6, 268–278. doi:10.1556/1846.2016.00015

Chen, D., Qiao, X., Qiu, X., and Chen, J. (2009). Synthesis and Electrical Properties of Uniform Silver Nanoparticles for Electronic Applications. *J. Mater. Sci.* 44, 1076–1081. doi:10.1007/s10853-008-3204-y

Davis, R. D., Jacobs, M. I., Houle, F. A., and Wilson, K. R. (2017). Colliding-Droplet Microreactor: Rapid On-Demand Inertial Mixing and Metal-Catalyzed Aqueous Phase Oxidation Processes. *Anal. Chem.* 89, 12494–12501. doi:10.1021/acs.analchem.7b03601

Fang, W.-F., and Yang, J.-T. (2009). A Novel Microreactor with 3D Rotating Flow to Boost Fluid Reaction and Mixing of Viscous Fluids. *Sensors Actuators B: Chem.* 140, 629–642. doi:10.1016/j.snb.2009.05.007

Guo, W., Heeres, H. J., and Yue, J. (2020). Continuous Synthesis of 5-hydroxymethylfurfural from Glucose Using a Combination of AlCl3 and HCl as Catalyst in a Biphasic Slug Flow Capillary Microreactor. *Chem. Eng. J.* 381, 122754. doi:10.1016/j.cej.2019.122754

Gupta, M. K., Meng, F., Johnson, B. N., Kong, Y. L., Tian, L., Yeh, Y.-W., et al. (2015). 3D Printed Programmable Release Capsules. *Nano Lett.* 15, 5321–5329. doi:10.1021/acs.nanolett.5b01688

Hessel, V., Löwe, H., and Schönfeld, F. (2005). Micromixers-a Review on Passive and Active Mixing Principles. *Chem. Eng. Sci.* 60, 2479–2501. doi:10.1016/j.ces.2004.11.033

Inohara, K., Asano, S., Maki, T., and Mae, K. (2019). Synthesis of Small Lipid Nanoparticles Using an Inkjet Mixing System Aiming to Reduce Drug Loss. *Chem. Eng. Technol.* 42, 2061–2066. doi:10.1002/ceat.201900041

Mandrycky, C., Wang, Z., Kim, K., and Kim, D.-H. (2016). 3D Bioprinting for Engineering Complex Tissues. *Biotechnol. Adv.* 34, 422–434. doi:10.1016/j.biotechadv.2015.12.011

Mer, V. K. L. (1952). Nucleation in Phase Transitions. *Ind. Eng. Chem.* 44, 1270–1277. doi:10.1021/ie50510a027

Mitsudome, T., Arita, S., Mori, H., Mizugaki, T., Jitsukawa, K., and Kaneda, K. (2008a). Supported Silver-Nanoparticle-Catalyzed Highly Efficient Aqueous Oxidation of Phenylsilanes to Silanols. *Angew. Chem.* 120, 8056–8058. doi:10.1002/ange.200802761

Mitsudome, T., Mikami, Y., Funai, H., Mizugaki, T., Jitsukawa, K., and Kaneda, K. (2008b). Oxidant-Free Alcohol Dehydrogenation Using a Reusable Hydrotalcite-Supported Silver Nanoparticle Catalyst. *Angew. Chem. Int. Ed.* 47, 138–141. doi:10.1002/anie.200703161

Muranaka, Y., Nakagawa, H., Masaki, R., Maki, T., and Mae, K. (2017). Continuous 5-hydroxymethylfurfural Production from Monosaccharides in a Microreactor. *Ind. Eng. Chem. Res.* 56, 10998–11005. doi:10.1021/acs.iecr.7b02017

Nagasawa, H., Aoki, N., and Mae, K. (2005). Design of a New Micromixer for Instant Mixing Based on the Collision of Micro Segments. *Chem. Eng. Technol.* 28, 324–330. doi:10.1002/ceat.200407118

Schindelin, J., Arganda-Carreras, I., Frise, E., Kaynig, V., Longair, M., Pietzsch, T., et al. (2012). Fiji: An Open-Source Platform for Biological-Image Analysis. *Nat. Methods* 9, 676–682. doi:10.1038/nmeth.2019

Scholl, J. A., Koh, A. L., and Dionne, J. A. (2012). Quantum Plasmon Resonances of Individual Metallic Nanoparticles. *Nature* 483, 421–427. doi:10.1038/nature10904

Schwesinger, N., Frank, T., and Wurmus, H. (1996). A Modular Microfluid System with an Integrated Micromixer. *J. Micromech. Microeng.* 6, 99–102. doi:10.1088/0960-1317/6/1/023

Takano, Y., Kikkawa, S., Suzuki, T., and Kohno, J.-y. (2015). Coloring Rate of Phenolphthalein by Reaction with Alkaline Solution Observed by Liquid-Droplet Collision. *J. Phys. Chem. B* 119, 7062–7067. doi:10.1021/acs.jpcb.5b03233

Takesue, M., Tomura, T., Yamada, M., Hata, K., Kuwamoto, S., and Yonezawa, T. (2011). Size of Elementary Clusters and Process Period in Silver Nanoparticle Formation. *J. Am. Chem. Soc.* 133, 14164–14167. doi:10.1021/ja202815y

Watanabe, S., Ohsaki, S., Hanafusa, T., Takada, K., Tanaka, H., Mae, K., et al. (2017). Synthesis of Zeolitic Imidazolate Framework-8 Particles of Controlled Sizes, Shapes, and Gate Adsorption Characteristics Using a central Collision-type Microreactor. *Chem. Eng. J.* 313, 724–733. doi:10.1016/j.cej.2016.12.118

Wiktor, P., Brunner, A., Kahn, P., Qiu, J., Magee, M., Bian, X., et al. (2015). Microreactor Array Device. *Sci. Rep.* 5, 1–8. doi:10.1038/srep08736

Yamada, T., Fukuhara, K., Matsuoka, K., Minemawari, H., Tsutsumi, J. y., Fukuda, N., et al. (2016). Nanoparticle Chemisorption Printing Technique for Conductive Silver Patterning with Submicron Resolution. *Nat. Commun.* 7, 1–9. doi:10.1038/ncomms11402